A Monte Carlo investigation of optical pathlength in inhomogeneous tissue and its application to near-infrared spectroscopy

M Hiraoka†¶, M Firbank†, M Essenpreis†, M Cope†, S R Arridge‡, P van der Zee§ and D T Delpy†

† Department of Medical Physics and Bioengineering, University College London, Shropshire House, 11-20 Capper Street, London WC1E 6JA, UK
‡ Department of Computer Science, University College London, Gower Street, London WC1E 6BT, UK
§ Division of Physical Sciences, University of Hertfordshire, College Lane, Hatfield, Herts, AL10 9AB, UK

Abstract. In order to quantify near-infrared spectroscopic (NIRS) data on an inhomogeneous medium, knowledge of the contribution of the various parts of the medium to the total NIRS signal is required. This is particularly true in the monitoring of cerebral oxygenation by NIRS, where the contribution of the overlying tissues must be known. The concept of the time point spread function (TPSF), which is used extensively in NIRS to determine the effective optical pathlength, is expanded to the more general inhomogeneous case. This is achieved through the introduction of the partial differential pathlength, which is the effective optical pathlength in the inhomogeneous medium, and an analytical proof of the applicability of the modified Beer–Lambert law in an inhomogeneous medium is shown. To demonstrate the use of partial differential pathlength, a Monte Carlo simulation of a two-concentric-sphere medium representing a simplified structure of the head is presented, and the possible contribution of the overlying medium to the total NIRS signal is discussed.

1. Introduction

In the past ten years, the technique of near infrared spectroscopy (NIRS) has been increasingly used to monitor blood and tissue oxygenation in patients, especially the status of the brain. In order to quantitate NIRS data, it is necessary to know the optical pathlength of the light in the tissue, which, due to the high degree of light scattering that occurs, is considerably greater than the geometrical spacing between the light input and output points. It has however been widely accepted that the detected signal is representative of the average oxygenation of the tissues between the optodes. This is a reasonable assumption when the tissues are homogeneous, but in the case of the head, the tissue of interest, the brain, lies below a surface layer of tissue and bone. In this paper, we report on the results of a Monte Carlo (MC) simulation of light transport in a heterogeneous structure comprising two concentric spheres, which represent in a simplistic manner the structure of the head. From these results we discuss the probable contribution of the overlying tissues to the detected NIRS signal. A theoretical basis for quantitation of optical pathlength in an inhomogeneous medium is also given.

¶ Present address: Fuji Electric Corporate R&D Ltd, 2-2-1 Nagasaka, Yokosuka shi, 240-01 Japan.

2. Near-infrared spectroscopy

The relative transparency of biological tissues to NIR light allows the absorption properties of intact organs to be monitored non-invasively. In the NIR, absorption due to haemoglobin and cytochrome oxidase can be observed, making it possible to monitor changes in blood and tissue oxygenation. The method was first applied to the brain of cats (Jöbsis 1977) and subsequently to the brains of newborn infants (Brazy *et al* 1985, Ferrari *et al* 1986a, Wyatt *et al* 1986) and adults (Ferrari *et al* 1986b, Fox *et al* 1985). Recently, methods for the absolute quantitation of cerebral blood flow and blood volume have been developed and applied to the newborn infant (Edwards *et al* 1988, Wyatt *et al* 1990, Skov *et al* 1991) and adult (Elwell *et al* 1992). The possibility of imaging of tissue oxygenation by NIR light is also being studied by various groups (Arridge *et al* 1991, 1993a, Fishkin and Gratton 1993, Knüttel *et al* 1993, Hebden and Wong 1993).

Quantitation of spectroscopy data using the Beer–Lambert law requires that the optical pathlength is known. In NIRS, light scattering by the tissues means that not all the light that enters the tissues is detected, and even that light has travelled along a distribution of paths. It has however previously been shown that a modified Beer–Lambert law can be applied to quantify *changes* in chromophore concentration from the measured *changes* in tissue attenuation (Delpy *et al* 1988, Cope *et al* 1988, Cope 1991). This modified law uses the differential pathlength (DP), which is defined as the local gradient of the attenuation versus the absorption coefficient μ_a of tissue. It has been shown experimentally that the DP can be approximated by measuring the mean distance $\langle L \rangle$ travelled across the tissue by picosecond light pulses (Delpy *et al* 1988) or by measuring the phase shift of a frequency modulated light source (Chance *et al* 1990) and the theoretical basis of both has been demonstrated by Arridge *et al* (1992). The differential pathlength factor (DPF), which is obtained when the DP is divided by the distance between light source and detector optodes, has been shown to be approximately constant once the optode spacing exceeds 2.5 cm (van der Zee *et al* 1990, van der Zee 1993).

Thus far, the use of the differential pathlength has only been demonstrated to be valid for a homogeneous medium, but real organs consist of various tissue components that have different optical parameters. Therefore, for the purpose of accurate quantitation of NIRS data it is important to understand the nature of light transport through an inhomogeneous medium and to know the effective optical pathlengths within the various parts of an inhomogeneous medium.

There are various methods for calculating light transport through tissue and a useful review is given by Patterson *et al* (1991). One approach is to seek an analytical solution of the diffusion equation. However, this has only succeeded under restricted geometries and for a homogeneous medium (Patterson *et al* 1988, Arridge *et al* 1992). A second approach is the MC method (Wilson and Adam 1983, van der Zee and Delpy 1987, Flock *et al* 1989, Sevick and Chance 1991, Essenpreis *et al* 1991), which can be applied to an inhomogeneous medium, has the advantage of being able to calculate the pathlength directly and can offer the individual photon histories, but which requires considerable computation time. A third approach is to solve the diffusion equation numerically by the finite-difference method (Cui and Ostrander 1992, Haselgrove *et al* 1992), which has been successful under restricted conditions for an inhomogeneous medium. A fourth approach is to solve the diffusion equation by the finite-element method (Schweiger *et al* 1992, Arridge *et al* 1993b), which can be applied to the complex geometries of an inhomogeneous medium and has the advantage of fast calculation time, but it does not calculate individual photon histories. We have chosen to use the MC method to calculate the DPs of an inhomogeneous medium.

3. Use of differential pathlength

In order to estimate the change $\Delta\mu_a$ of absorption coefficient in a scattering medium from a change ΔOD in the measured light attenuation, a modified Beer–Lambert law has been shown to be applicable (Delpy *et al* 1988).

$$\text{Attenuation (OD)} = -\ln(I/I_0) = \text{DP}\mu_a + G \tag{1}$$

$$\Delta\text{OD} \simeq \text{DP}\Delta\mu_a \tag{2}$$

where I_0 is the time averaged input light irradiance on the medium surface and I is the time averaged detected light irradiance on the medium surface. DP is the differential pathlength, which is a function of absorption coefficient μ_a, scattering coefficient μ_s, single-scattering phase function f_p and geometry. G is another function, which depends on μ_s, f_p and geometry but not on μ_a. Strictly speaking equations (1) and (2) are only correct if DP does not depend on μ_a. Although this is not strictly true, in NIR tissue spectroscopy we normally only observe small changes of μ_a where DP has been shown to be approximately constant (Cope 1991).

In a homogeneous medium it has been shown experimentally that the DP can be approximated by the mean time $\langle T \rangle$ of the TPSF multiplied by the velocity c of light in the medium (Delpy *et al* 1988):

$$\text{DP} = \Delta\text{OD}/\Delta\mu_a \simeq c\langle T \rangle. \tag{3}$$

The TPSF is defined as the temporal intensity distribution of light emerging from the tissue following the input of an ultrashort light pulse. A typical TPSF profile for a homogeneous slab of scattering medium is shown in figure 1(*a*). Theoretical analysis using the diffusion approximation has also shown this relationship (Patterson *et al* 1989, Arridge *et al* 1992). A dimensionless factor, the DPF, is sometimes used in NIRS and is defined as (Delpy *et al* 1988)

$$\text{DPF} = \text{DP}/D \tag{4}$$

where D is the distance between the light source and detector optodes. The DPF indicates how many times longer the detected light has travelled than the interoptode spacing.

4. Relationship between DP and $\langle T \rangle$ in a heterogeneous medium

In discussing a heterogeneous medium, we will introduce the concepts of the partial differential pathlength (PDP) and the partial mean time of the TPSF defined later in (5) and (13) respectively, and will show that a similar relationship exists between these parameters. The proof will not depend on the diffusion approximation.

Consider a heterogeneous medium which consists of n separate components of any geometry. Suppose that each component of the medium is homogeneous but has different optical properties. We define the PDP as a partial derivative of the measured attenuation OD versus the absorption coefficient μ_{ai}, $i = 1, \ldots, n$, of each medium.

$$\text{PDP}_i = \partial\text{OD}/\partial\mu_{ai}. \tag{5}$$
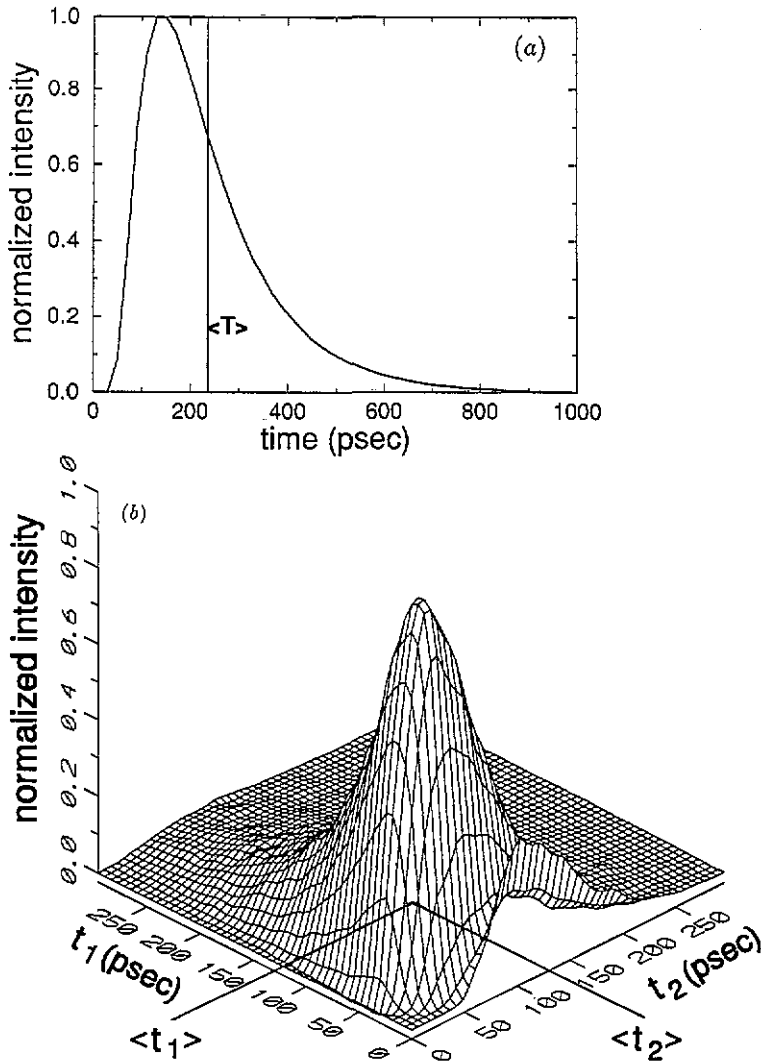
Figure 1. A typical TPSF showing the mean time (T) calculated by the MC model (a) for photons transmitted through a homogeneous slab medium (the thickness of the slab is 10 mm, $\mu'_s = 1$ mm^{-1} and $\mu_a = 0.01$ mm^{-1}) and (b) for transmission through a heterogeneous concentric sphere medium that consists of two components (the diameter of the outer sphere is 20 mm and that of the inner sphere 16 mm; the inner medium (medium 1) has $\mu'_{s1} = 0.5$ mm^{-1} and $\mu_{a1} = 0.02$ mm^{-1}; the outer medium (medium 2) has $\mu'_{s2} = 2$ mm^{-1} and $\mu_{a2} = 0.02$ mm^{-1}; the input/output optode angle Θ is 60°; t_1 is the time spent in the medium 1 and t_2 is the time in the medium 2).

Hence, substituting for OD

$$\text{PDP}_i = (\partial/\partial\mu_{ai}[-\ln(I/I_0)] = -(1/I)\partial I/\partial\mu_{ai}. \tag{6}$$

Any photon arriving at the surface at time T can be associated with a vector $(t_1, t_2, \ldots, t_n)$, where t_1, $i = 1, \ldots, n$, is the time spent within the medium i. We may then define a function $P(t_1, t_2, \ldots, t_n)$ that represents the intensity of photons received with a particular distribution of component times. $P(t_1, t_2, \ldots, t_n)$ may have a value for $t_i \geqslant 0$ and is equal

to zero for any $t_i < 0$. Figure 1(*b*) shows an example of this function for a two-component-concentric-sphere medium. This may be called the TPSF for an inhomogeneous medium. Note that in figure 1(*b*) we may take a diagonal line $t_1 + t_2 = T$ and perform the integral

$$\Gamma(T) = \int_0^\infty P(t_1, T - t_1) \, dt_1. \tag{7}$$

to recover our normal definition of received intensity, which is the TPSF for T. In general

$$\Gamma(T) = \int_0^\infty \cdots \int_0^\infty P\left(t_1, t_2, \ldots, t_{n-1}, T - \sum_{i=1}^{n-1} t_i\right) dt_1 \, dt_2 \ldots dt_{n-1}. \tag{8}$$

The function $P(t_1, t_2, \ldots, t_n)$ and $\Gamma(T)$ if normalized may also be regarded as the probability density function for the transit times of the photons.

Let $P_0(t_1, t_2, \ldots, t_n)$ be the TPSF in the case of a non-absorbing medium ($\mu a_i = 0$, $i = 1, \ldots, n$). Then absorption may be introduced by multiplying $P_0(t_1, t_2, \ldots, t_n)$ by the probability that a photon remains unabsorbed in the medium i, which is $\exp(-\mu_{ai} c_i t_i)$, where c_i is the velocity of light in the medium i. In other words, the received intensity of any given photon will be attenuated by a factor $\exp(-\mu_{ai} c_i t_i)$ for any non-zero attenuation in the medium i, so that the total attenuation for the photons received with a particular distribution of component times is

$$P(t_1, t_2, \ldots, t_n) = P_0(t_1, t_2, \ldots, t_n) \prod_{i=1}^n \exp(-\mu_{ai} c_i t_i) = P_0(t_1, t_2, \ldots, t_n)$$

$$\times \exp\left(-\sum_{i=1}^n (\mu_{ai} c_i t_i)\right). \tag{9}$$

Then the measured intensity I is the integral of $P_0(t_1, t_2, \ldots, t_n)$ over time

$$I = \int_0^\infty \cdots \int_0^\infty P(t_1, t_2, \ldots, t_n) \, dt_1 \, dt_2 \ldots dt_n$$

$$= \int_0^\infty \cdots \int_0^\infty P_0(t_1, t_2, \ldots, t_n) \exp\left(-\sum_{i=1}^n (\mu_{ai} c_i t_i)\right) dt_1 \, dt_2 \ldots dt_n. \tag{10}$$

Also

$$\frac{\partial I}{\partial \mu_{ai}} = -c_i \int_0^\infty \cdots \int_0^\infty t_i P_0(t_1, t_2, \ldots, t_n) \exp\left(-\sum_{i=1}^n (\mu_{ai} c_i t_i)\right) dt_1 \, dt_2 \ldots dt_n \tag{11}$$

so that:

$$\text{PDP}_i = -\frac{1}{I} \frac{\partial I}{\partial \mu_{ai}} = c_i \int_0^\infty \cdots \int_0^\infty t_i P_0(t_1, t_2, \ldots, t_n) \exp\left(-\sum_{i=1}^n (\mu_{ai} c_i t_i)\right) dt_1 \, dt_2 \ldots dt_n$$

$$\Big/ \int_0^\infty \cdots \int_0^\infty P_0(t_1, t_2, \ldots, t_n) \exp\left(-\sum_{i=1}^n (\mu_{ai} c_i t_i)\right) dt_1 \, dt_2 \ldots dt_n. \tag{12}$$

On the other hand, the partial mean time $\langle t_1 \rangle$ of the TPSF, which is defined as the mean time spent within the medium i, is given by

$$\langle t_1 \rangle = \int_0^\infty \cdots \int_0^\infty t_i P(t_1, t_2, \ldots, t_n) \, dt_1 \, dt_2 \ldots dt_n$$

$$\Bigg/ \int_0^\infty \cdots \int_0^\infty P(t_1, t_2, \ldots, t_n) \, dt_1 \, dt_2 \ldots dt_n$$

$$= \int_0^\infty \cdots \int_0^\infty t_i P_0(t_1, t_2, \ldots, t_n) \exp\left(-\sum_{i=1}^n (\mu_{ai} c_i t_i)\right) dt_1 \, dt_2 \ldots dt_n$$

$$\Bigg/ \int_0^\infty \cdots \int_0^\infty P_0(t_1, t_2, \ldots, t_n) \exp\left(-\sum_{i=1}^n c_i t_i\right) dt_1 \, dt_2 \ldots dt_n \qquad (13)$$

and the mean $\langle T \rangle$ of total transit time is

$$\langle T \rangle = \int_0^\infty T \Gamma \langle T \rangle \, dT \Bigg/ I$$

$$= \int_0^\infty T \, dT \int_0^\infty \cdots \int_0^\infty P\left(t_1, \ldots, t_{n-1}, T - \sum_{i=1}^{n-1} t_i\right) dt_1 \ldots dt_{n-1} \Bigg/ I$$

$$= \int_0^\infty \cdots \int_0^\infty \left[t_1 + \ldots + t_{n-1} + \left(T - \sum_{i=1}^{n-1} t_i\right)\right]$$

$$\times P\left(t_1, \ldots, t_{n-1}, T - \sum_{i=1}^{n-1} t_i\right) dt_1 \ldots dt_{n-1} \, dT \Bigg/ I$$

$$= \int_0^\infty \cdots \int_0^\infty (t_1 + \cdots + t_{n-1} + t_n) P(t_1, \ldots, t_{n-1}, t_n) \, dt_1 \ldots dt_{n-1} \, dt_n \Bigg/ I$$

$$= \sum_{i=1}^n \langle t_i \rangle. \qquad (14)$$

Comparing (12) to (13), we obtain

$$\text{PDP}_i = \partial \text{OD}/\partial \mu_{ai} = c_i \langle t_i \rangle. \qquad (15)$$

(15) shows that the PDP_i is exactly equal to the mean time $\langle t_i \rangle$ in the medium i multiplied by the velocity c_i of light in the medium i. Therefore PDP_i is equal to the mean pathlength $\langle L_i \rangle$ of the light travelling within the medium i

$$\text{PDP}_i = \langle L_i \rangle. \qquad (16)$$

(Note that we are not dealing with all the photons in the medium but only those photons that arrive at the exit point.) Then the total attenuation change is

$$\Delta\text{OD} = \sum_{i=1}^n \left(\frac{\partial \text{OD}}{\partial \mu_{ai}} \Delta\mu_{ai}\right) \qquad (17a)$$

$$= \sum_{i=1}^n (\text{PDP}_i \Delta\mu_{ai}) = \sum_{i=1}^n (\langle L_i \rangle \Delta\mu_{ai}). \qquad (17b)$$
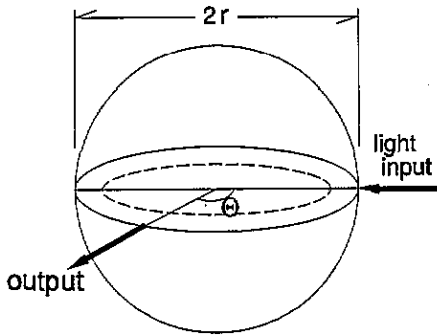
Figure 2. Geometry for the MC model. The boundaries of the heterogeneous medium are two concentric spheres. The exit position is specified by the angle Θ.

(17) means that the modified Beer–Lambert law is still applicable to each of the components of the heterogeneous medium, and the total attenuation change is the sum of the attenuation changes of each component. Note that we could have derived (17a) by assuming that OD is function of $(\mu_{a1}, \mu_{a2}, \ldots, \mu_{an})$ and using the Taylor series. However, this would not allow us to state (17b).

It is useful to define a dimensionless factor, the partial differential pathlength factor (PDPF), in the same way as for the homogeneous medium:

$$\text{PDPF}_i = \text{PDP}_i/D = \langle L_i \rangle/D \tag{18}$$

where D is the geometric distance between the light source and detector optode.

Furthermore, it is interesting to note that the way PDP varies as a function of the absorption coefficients can be expressed as follows:

$$\partial \text{PDP}_i/\partial \mu_{ai} = -\text{Var}(L_i) \tag{19}$$

where $\text{Var}(L_i)$ is the variance of the pathlengths in the medium i. Equation (19) can easily be derived from (12).

In order to determine the $\Delta \mu_a$ of each medium, we need to know ΔOD and PDP for each medium, but current experimental techniques only allow us to measure the total ΔOD and $\langle T \rangle$. Although it is difficult to measure PDP experimentally, computation techniques such as MC modelling can provide this information.

5. Monte Carlo model

5.1. Model

Figure 2 shows the geometry of the MC model. This consists of two homogeneous components, the boundaries of which are two concentric spheres. Each component is characterized by its optical parameters, i.e. absorption coefficient μ_{a1}, μ_{a2}, scattering coefficient μ_{s1}, μ_{s2} and single-scattering phase function $f_1(\theta)$, $f_2(\theta)$, (the subscript 1 represents the inner medium and the subscript 2 represents the outer medium). Refractive indexes of the media are assumed to be the same. The model calculates the total mean pathlength (the differential pathlength, DP), the mean pathlength in each medium (the partial differential pathlength, PDP) and estimates the contribution of the outer medium to the change ΔOD of the total optical density.

Photons with the initial weight of one are introduced perpendicular to the medium surface, and for each the path of the photon is first calculated without considering absorption. Once the photon exits from the medium surface, absorption is introduced by weighting each detected photon. Some details of the model as applied to a homogeneous medium have been given previously (van der Zee 1993), but brief details of its application to the heterogeneous case are given here.

Successive scattering lengths l_i in medium i are calculated as $l_i = -\ln(R)/\mu_{si}$, where μ_{si} is the scattering coefficient of the medium i and R is a random number between 0 and unity. If a photon crosses the boundary from medium i to medium j, the scattering length l_j in the medium j is recalculated as $l_j = (\mu_{si}/\mu_{sj})l'_j$, where μ_{sj} is the scattering coefficient of medium j and l'_j is the scattering length in the medium j in the case where $\mu_{sj} = \mu_{si}$.

Reflection and refraction of light at the boundary between air and tissue is taken into account. If photons reach the medium surface, the path of the photon is split into two directions according to Snell's law. One photon exits from the surface with weight W_0, which is calculated by Fresnel's law, the other, which has the residual weight $(1 - W_0)$, returning into the medium where it travels until its energy weight becomes negligible. The boundary is regarded as an ideal smooth surface. The photon exit position is described by the angular position Θ on the sphere.

For each output photon, the pathlengths L_1 and L_2 in the inner medium and outer medium respectively are calculated by accumulating the scattering lengths in each medium, $L_i = \sum l_i$. Absorption is introduced by considering the probability that a photon remains unabsorbed in the medium i to be $\exp(\mu_{ai}L_i)$, thus the weight W for an exit photon is

$$W = W_0 \exp\left(-\sum_{i=1}^{2}(\mu_{ai}L_i)\right) \tag{20}$$

where W_0 is the weight of the exit photon in the zero-absorption case and is equal to unity if there is no reflection and refraction at the boundary.

The model records a set of values $(\sum W|_{\Theta \pm \Delta\Theta}, \sum\{L_1 W\}|_{\Theta \pm \Delta\Theta}, \sum\{L_2 W\}|_{\Theta \pm \Delta\Theta})$ for each exit position Θ, where $|_{\Theta \pm \Delta\Theta}$ indicates the range of accumulation over the exit position between $\Theta - \Delta\Theta$ and $\Theta + \Delta\Theta$ (i.e. an annular ring). The light intensity $I(\Theta)$ at exit position Θ for continuous wave incident light is calculated as

$$I(\Theta) = \frac{I}{N}\sum W|_{\Theta \pm \Delta\Theta} \tag{21}$$

where N is the number of input photons. The partial differential pathlength $\mathrm{PDP}_i(\Theta)$ of medium i for exit position Θ is calculated as

$$\mathrm{PDP}_i(\Theta) = \langle L_i(\Theta)\rangle = \sum(L_i W)|_{\Theta \pm \Delta\Theta}\Big/\sum W|_{\Theta \pm \Delta\Theta}. \tag{22}$$

This equation corresponds to (12) in section 4. The partial differential pathlength factor $\mathrm{PDPF}_i(\Theta)$ of medium i for exit position Θ is calculated as PDP_i divided by chord length

$$\mathrm{PDPF}_i(\Theta) = \mathrm{PDP}_i(\Theta)/\mathrm{chord}(\Theta) = \mathrm{PDP}_i(\Theta)/2r\sin(\Theta/2) \tag{23}$$

where r is the radius of the sphere.

The model was initially run to provide data to validate the applicability of the modified Beer–Lambert law in an inhomogeneous medium, i.e. to look at the variation of $\Delta\mathrm{OD}$ versus

$\sum(\langle L_i \rangle \Delta\mu_{ai})$. Secondly, two runs were performed with the same model to compare the variation of DPF with Θ for the cases of non-isotropic scattering and isotropic scattering using a transport scattering coefficient $\mu'_s = \mu_s(1-g)$, where g is the mean cosine of the single-scattering phase function. If these results are identical, the MC calculation can be speeded up by using an isotropic scattering assumption. Finally the model was run while altering the optical properties of the outer medium to investigate the effect of the outer medium on the DP.

5.2. Parameters of the model

The parameters and the values used in the MC model are listed in table 1. The outside diameter $(2r)$ is 30 mm and the distance ξ between spheres is 2 mm. The size of this sphere is small in order to keep the computation time within reasonable limits. Although this is much smaller than the adult head, the ratio of the sphere diameters has been chosen to be comparable to the ratio of the thickness of the skin and skull to the overall head diameter.

Table 1. Parameters of the model.

Sphere diameter	30 mm
Thickness of skin + skull annulus	2 mm
Refractive index of tissue	1.4
Absorption coefficient (inside medium)	0.01 mm^{-1}
(outside medium)	0.001–0.1 mm^{-1}
Scattering coeffcient (inside medium)	9 mm^{-1}
(outside medium)	1.8–18 mm^{-1}
Number of output photons (all surfaces)	10 million

Over the past few years, a number of investigators have reported data on the optical properties of various tissues and a comprehensive review of these can be found in the article by Cheong *et al* (1990). In our model, we have used as optical properties for the inside medium $\mu'_s = \mu_s(1-g) = 9$ mm^{-1}, $\mu_a = 0.01$ mm^{-1} (adult brain white matter at wavelength 750 nm) and a measured scattering phase function with $g = 0.81$ (adult brain white matter, average for wavelength 550–900 nm, van der Zee 1993). For the outer medium, a range of values has been modelled including $\mu'_s = 2$ mm^{-1}, $\mu_a = 0.02$ mm^{-1} (pig skull at wavelength 750 nm) with a measured scattering phase function with $g = 0.93$ (pig skull at wavelength 800 nm, Firbank *et al* 1993) and $\mu'_s = 2.5$ mm^{-1}, $\mu_a = 0.04$ mm^{-1} (adult brain grey matter, van der Zee 1993).

6. Results

In figure 3, the sum $\sum(\langle L_i \rangle \Delta\mu_{ai})$ of the PDPs multiplied by changes of the absorption coefficient of each medium is plotted against the total attenuation change ΔOD for different exit angles Θ. The modelled ranges of both the absorption coefficient μ_{a1} of the inside medium and the absorption coefficient μ_{a2} of the outside medium are 0.005, 0.01, 0.02, 0.04, 0.07, 0.1 mm^{-1} and the corresponding values of $\Delta\mu_{ai}$ are the intervals between μ_{ai} and the next μ_{ai}. For all combinations of (μ_{a1}, μ_{a2}), the corresponding ΔOD and $\sum(\langle L_i \rangle \Delta\mu_{ai})$
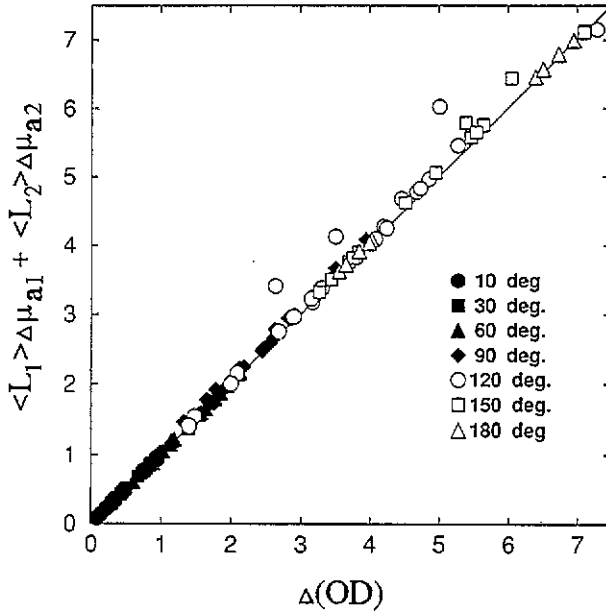
Figure 3. The sum $\sum(\langle L_i \rangle \Delta \mu_{ai})$ of the PDP multiplied by changes of the absorption coefficients versus the attenuation change ΔOD for different exit angles Θ $10° = (\bullet)$, $30° = (\blacksquare)$, $60° = (\blacktriangle)$, $90° = (\blacklozenge)$, $120° = (\bigcirc)$, $150° = (\square)$ and $180° = (\triangle)$. The diameter of the outer sphere is 30 mm and that of the inner sphere is 26 mm. The inner medium (medium 1) has $\mu'_{s1} = 9$ mm^{-1}, $g = 0.81$, and the outer medium (medium 2) has $\mu'_{s2} = 2$ mm^{-1}, $g = 0.93$. Ranges of both μ_{a1} and μ_{a2} are 0.005, 0.01, 0.02, 0.04, 0.07, 0.1 mm^{-1} and the corresponding values of $\Delta \mu_{ai}$ are the intervals between μ_{ai} and the next μ_{ai}. For all combinations of (μ_{a1}, μ_{a2}), the corresponding ΔOD and $\sum(\langle L_i \rangle \Delta \mu_{ai})$ were calculated. The line of identity is also shown.

were calculated, the photons being collected within annular rings $\Theta \pm 5°$. Five million photons were traced.

Figure 4 shows a comparison of the DPF and the partial differential pathlength factor PDPF$_2$ of the outside medium as a function of the exit angle, calculated using either an isotropic scattering model (solid line) or a non-isotropic scattering model (dotted line). Both models had the same transport scattering coefficients and absorption coefficients. In the non-isotropic case, the inner medium used $\mu_{s1} = 47.4$ mm^{-1} and $g = 0.81$ (i.e. $\mu'_{s1} = 9$ mm^{-1}) and for the outer medium $\mu'_{s2} = 28.6$ mm^{-1}, $g = 0.93$ (i.e. $\mu'_{s2} = 2$ mm^{-1}). Five million photons were traced. The corresponding values for the isotropic case are $\mu_{s1} = 9$ mm^{-1} ($g = 0$) for the inner medium, $\mu_{s2} = 2$ mm^{-1} ($g = 0$) for the outer medium, and twenty million photons were traced. In both cases for the inner medium $\mu_{a1} = 0.04$ mm^{-1} and for the outer medium $\mu_{a2} = 0.01$ mm^{-1}. The photons are collected within the annular rings and the exit angles Θ are specified by the centre of the corresponding intervals.

In figures 5, 6 and 7, the partial differential pathlengths PDP$_1$ and PDP$_2$ of the inner medium and outer medium respectively, the total DP and the ratio of PDP$_1$/DP are plotted as a function of μ_{a2}/μ_{a1} for different μ'_{s2}/μ'_{s1}. Figure 5 shows results for the exit angle $\Theta = 30°$, figure 6 for $\Theta = 45°$ and figure 7 for $\Theta = 75°$. In these figures μ_{a1} is fixed at 0.01 mm^{-1} and μ'_{s1} is fixed at 9 mm^{-1}; an isotropic scattering phase function was used. The photons are collected within the annular rings $\Theta \pm 5°$. Ten million photons were traced.
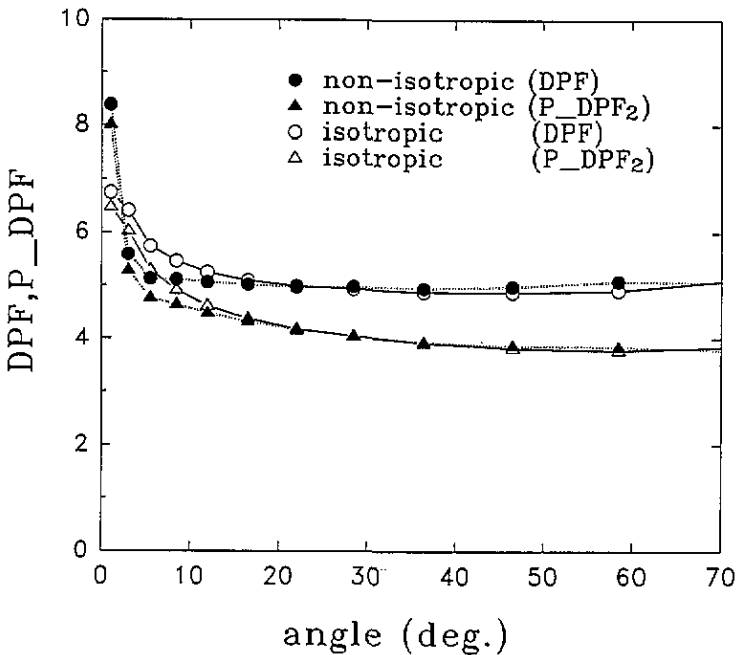
Figure 4. Comparison of the DPF ($\bullet$, $\bigcirc$) and the PDPF of the outer medium ($\blacktriangle$, $\triangle$) calculated using an isotropic (solid line) and a non-isotropic scattering model (dotted line) as a function of the exit angle Θ. Both models use the same transport scattering coefficients and absorption coefficients. In the non-isotropic case, the inner medium $\mu_s' = 9$ mm^{-1} and $g = 0.81$; for the outer medium $\mu_s' = 2$ mm^{-1} and $g = 0.93$. The corresponding values for the isotropic case are $\mu_s' = 9$ mm^{-1} ($g = 0$) for the inner medium, $\mu_s' = 2$ mm^{-1} ($g = 0$) for the outer medium. In both cases for the inner medium $\mu_a = 0.04$ mm^{-1} and for the outer medium $\mu_a = 0.01$ mm^{-1}.

7. Discussion

The validity of the modified Beer–Lambert law (17) in the case of an inhomogeneous medium is demonstrated by the linear relationship (figure 3) between the attenuation change ΔOD and $\sum(\langle L_i \rangle \Delta \mu_{ai})$. The data show some variation around the line of identity but this is due to statistical error of the MC simulation.

Figure 4 shows that in the case of large input/output separations, it is justifiable to use an isotropic phase function and the transport scattering coefficient μ_s' instead of the measured tissue phase functions and scattering coefficient μ_s and hence to reduce the computation time needed for these simulations. In the figure the DPF and the PDPF of the outer medium are calculated using both isotropic and non-isotropic scattering phase functions. The two sets of data only differ significantly when the detector position is close to the light input position (i.e. the angle is < 15°). It is interesting to note that in these data, the PDPF and DPF increase at short input/output positions (i.e. at small angles). Both MC calculations based upon a homogeneous sphere model (van der Zee *et al* 1990) and the analytical solution of the diffusion equation for a homogeneous sphere (Arridge *et al* 1992) predict the opposite behaviour, i.e. DPF falling with decrease in Θ. However, experimental data for several tissues including the adult head (van der Zee *et al* 1992) do show the type of rise predicted by these new calculations on an inhomogeneous sphere.
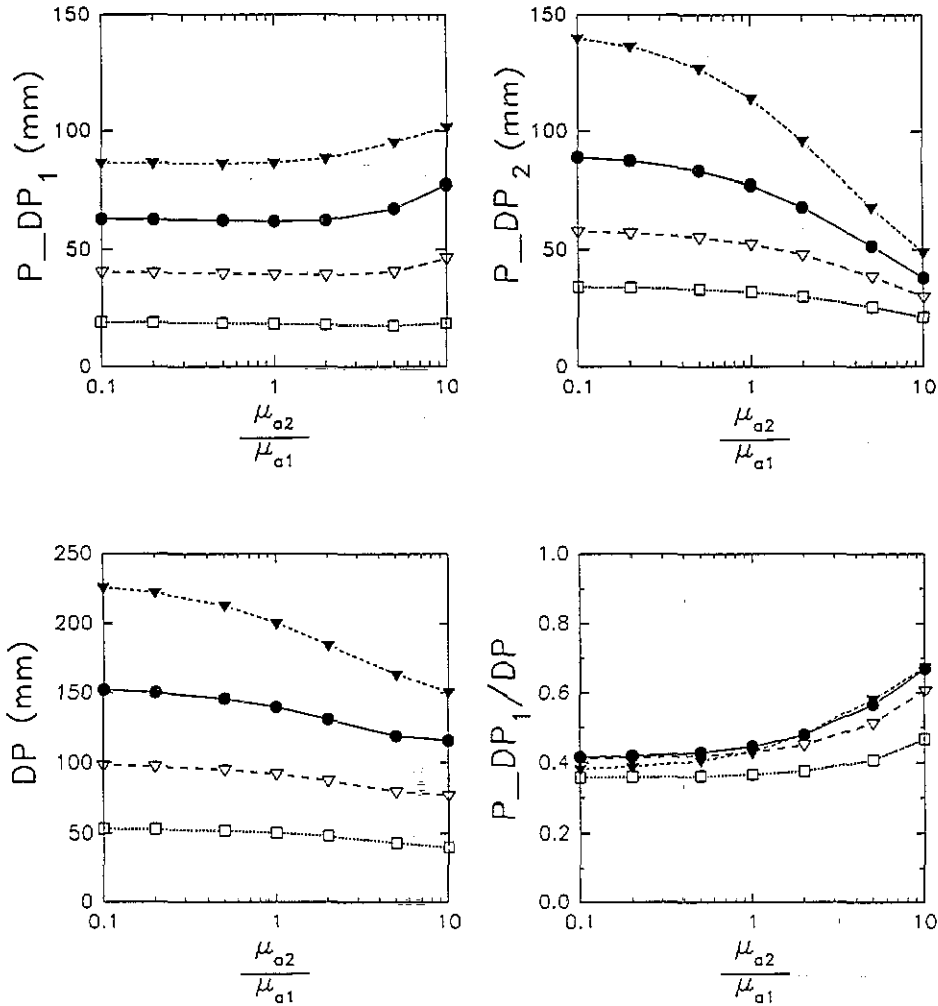
Figure 5. The partial differential pathlength PDP$_1$ of the inner medium, the PDP$_2$ of the outer medium, the DP and PDP$_1$/DP plotted as a function of μ_{a2}/μ_{a1} for different cases of μ'_{s2}/μ'_{s1} at an exit angle $\Theta = 30°$. μ_{a1} is fixed at 0.01 mm^{-1} and μ'_{s1} is fixed at 9 mm^{-1}. An isotropic scattering phase function was used. μ'_{s2}/μ'_{s1}: ▼, 2.0; ●, 1.0; ▽, 0.5; □, 0.2.

The effects of overlying tissue on the total effective optical pathlength for the two-concentric-sphere model are shown in figures 5, 6 and 7 for input/output angles of 30°, 45° and 75°, respectively. In NIR measurements on the human head, the distance between the optodes is typically about 4–6 cm. This means that the angle Θ between the optodes in measurements on the adult head (16 cm in diameter) is about 30–45° and that on the full-term baby head (10 cm diameter) is about 45–75°.

When we look at the results for the exit angles $\Theta = 30°$, 45° and 75°, the ratio PDP$_1$/DP of the inner PDP to the total DP is relatively constant as the scattering coefficient μ'_{s2} of the outer medium is altered and it slightly increases when the absorption coefficient μ_{a2} of the outer medium increases. Both PDP$_1$ and PDP$_2$ increase when μ'_{s2} increases (therefore the total DP also increases.) However, PDP$_2$ decreases when μ_{a2} increases and PDP$_1$ increases
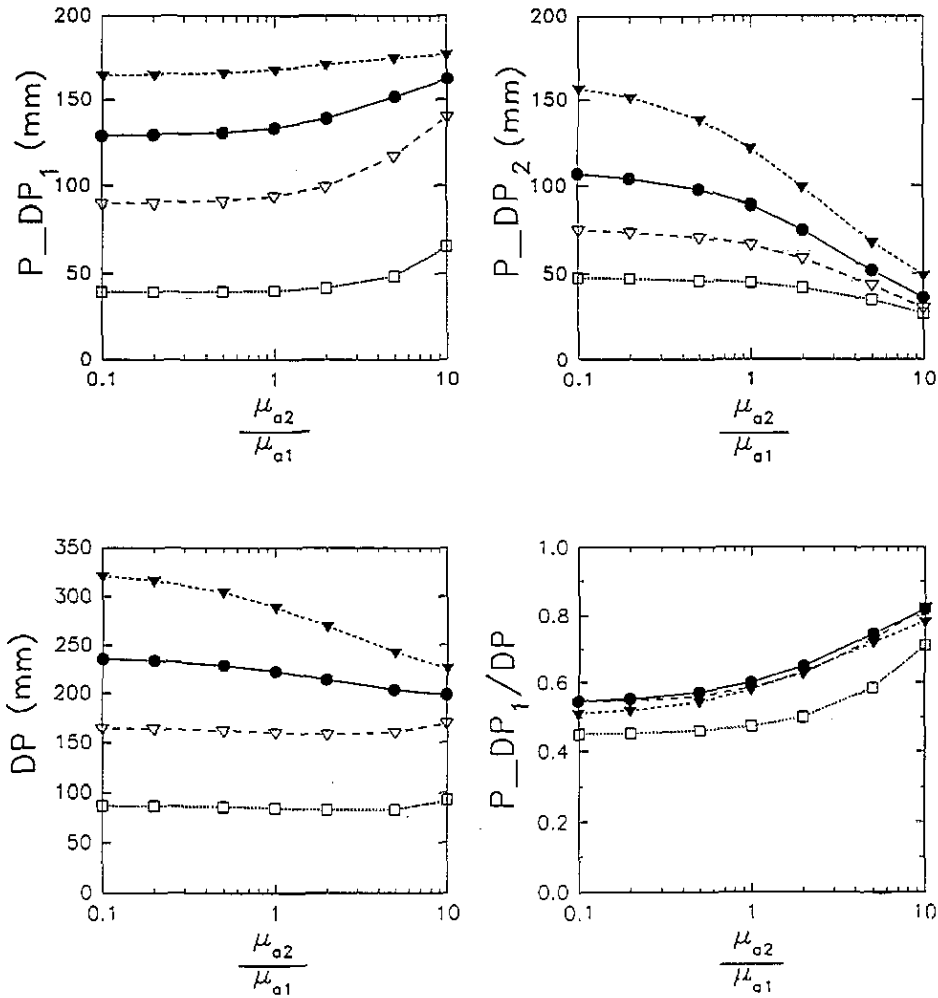
Figure 6. As figure 5, with $\Theta = 45°$.

slightly when μ'_{a2} increases. The ratio of PDP$_1$ to DP also increases as the exit position (angle Θ) increases. Although we have no analytical argument for this observation, an intuitive explanation for these results is as follows.

When μ'_{s2} is small, the photons that have only travelled in the outer medium are not scattered many times (i.e. 'short-cut' path photons exist) so the mean pathlength in the outer medium is relatively short. The intensity weight of these photons is correspondingly large and some of them can graze the inner medium without significant decrease of their intensity weight. When μ'_{s2} increases, the photons passing through the outer medium and grazing the inner medium are scattered more times and their intensity weight decreases, therefore the mean pathlengths PDP$_2$ and PDP$_1$ of both the outer medium and the inner medium, respectively, increase. This possibility has been examined by comparing the TPSF profiles for the case $\mu_{s2}/\mu_{s1} = 1$ (figure 8(a)) and the case $\mu_{s2}/\mu_{s1} = 0.2$ (figure 8(b)). Both figures use $\mu_{a1} = \mu_{a2} = 0$ and $\Theta = 60°$; t_1 is the time spent in the inner medium and t_2 is the time in the outer medium. In figure 8(b) there is a peak near the axis origin, which
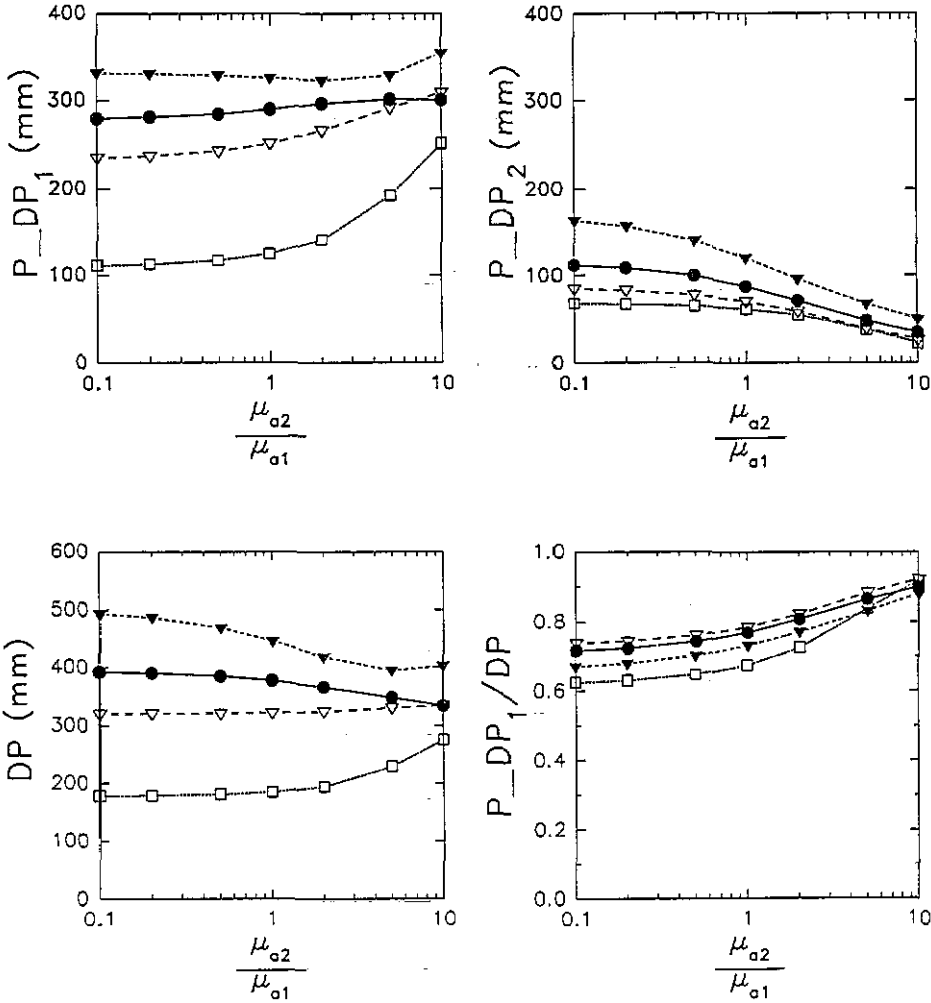
Figure 7. As figure 5, with $\Theta = 75°$.

corresponds to the 'short-cut' path photons, but this disappears in figure 8(a).

When considering the effect of changes in μ_{a2} upon the PDP, the following equations can be derived for a two-component medium from (9):

$$\partial DP/\partial \mu_{a2} = \partial PDP_2/\partial \mu_{a2} + \partial PDP_1/\partial \mu_{a2}$$

$$\partial PDP_2/\partial \mu_{a2} = -Var(L_2) \tag{24}$$

$$\partial PDP_1/\partial \mu_{a2} = -Cov(L_1, L_2)$$

where $Var(L_2)$ is the variance of the pathlengths in the outer medium and $Cov(L_1, L_2)$ is the covariance between the pathlengths L_1 and L_2 in the inner and the outer medium, respectively. $Var(L_2)$ must always be larger than zero so that PDP$_2$ will decrease when μ_{a2} increases. $Cov(L_1, L_2)$ can be either positive or negative, but the nearly symmetric TPSF
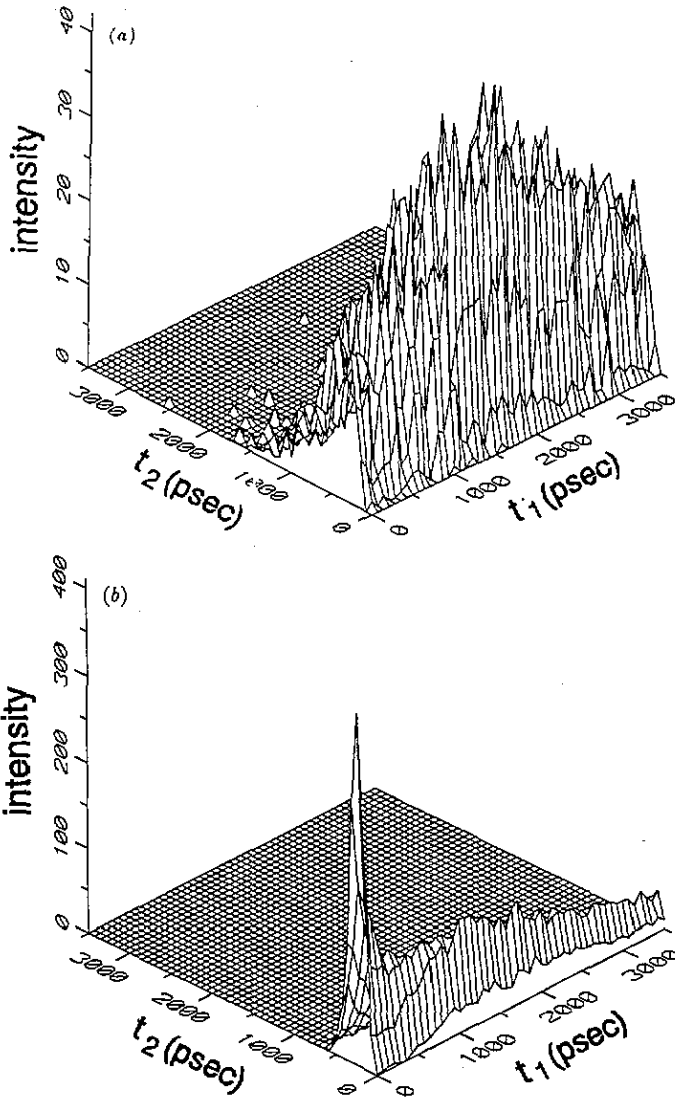
Figure 8. The TPSF of the two-concentric-sphere model: (a) $\mu'_{s2}/\mu'_{s1} = 1$; (b) $\mu'_{s2}/\mu'_{s1} = 0.2$. In both graphs the diameter of the outer sphere is 30 mm, that at the inner sphere is 26 mm, $\mu'_{s1} = 9$ mm^{-1}, $\mu_{a1} = \mu_{a2} = 0$ mm^{-1}, $\Theta = 60°$, t_1 is the time spent in the inner medium and t_2 is the time in the outer medium.

profiles (figure 8) show that $\text{Cov}(L_1, L_2)$ is nearly zero when $\mu_a = 0$. When μ_a increases, the weight of the photons that have travelled longer pathlength decreases exponentially so that the major axis of the TPSF distributions rotates clockwise. This means that $\text{Cov}(L_1, L_2)$ is likely to be negative, therefore PDP$_2$ increases when μ_{a2} increases. The PDP$_1$/DP ratio increases as μ_{a2} increases because PDP$_2$ decreases while PDP$_1$ increases. It can easily be seen from the geometry of the two concentric spheres that PDP$_1$/DP will increase as Θ increases.

In order to examine the consequences of this modelling upon NIRS of the adult and neonate head and to estimate accurately the effective optical pathlength of light in the

brain, we need to use an accurate forward model of light transport and require a complex description of the geometry of the head together with correct values for the optical properties of the head tissues. Compared to the ideal model, our two-concentric-sphere model is very simple; however, it can offer some approximate information about the likely NIR signal distributions.

If we use values of the adult brain white matter at wavelength 750 nm ($\mu'_s = 9$ mm^{-1}, $\mu_a = 0.01$ mm^{-1}) for the inner medium and those of the pig skull ($\mu'_s = 2$ mm^{-1}, $\mu_a = 0.025$ mm^{-1}) for the outer medium, the DPF is about six for an exit angle $\Theta = 30°$, about seven for $\Theta = 45°$ and about 12 for $\Theta = 75°$, and the ratio PDP$_1$/DP of the inner PDP to the total DP is about 40% for $\Theta = 30°$, about 55% for $\Theta = 45°$ and about 75% for $\Theta = 75°$. The experimentally measured DPF value for the adult head is about 6-7 at a wavelength of 750 nm for 4 cm input/output optode separation (i.e. $\Theta = 30°$) (Essenpreis *et al* 1993), therefore our calculated result for the DPF is very close.

If we use the values of the grey matter at a wavelength of 750 nm ($\mu'_s = 2.5$ mm^{-1}, $\mu_a = 0.04$ mm^{-1}) for the inner medium and the values of the pig skull for the outside medium, we may refer to the data point at $\mu_{a2}/\mu_{a1} = 0.625$ and $\mu'_{s2}/\mu'_{s1} = 0.8$. Here PDP$_1$/DP is still about 40% for $\Theta = 30°$, about 55% for $\Theta = 45°$ and about 75% for $\Theta = 75°$, similar to the results obtained using white matter as the inner medium.

This relative insensitivity to the μ_s ratio may imply that the effective pathlength PDP in the brain tissue may be about 40–55% of the total effective pathlength for an exit angle of 30–45° (adult brain measurement) and about 55–75% for an exit angle of 45–75° (baby head measurement).

As previously mentioned, the size of our model (30 mm diameter) is very small compared to the real human head. The problem of scaling has been reported in an infinite homogeneous slab medium by Graaff *et al* (1993). Their scaling relationship predicts that if the model was scaled to real size, the contribution of the overlying tissues to the total effective pathlength would increase. However, it is not clear whether this analysis can be applied to the heterogeneous spherical model used here. An alternative approach to this problem which we are currently pursuing is to use a finite-element model of light transport, which is a much faster simulation method.

Irrespective of the problems of scaling, the contribution of the overlying tissues to the total effective pathlength decreases as the exit angle increases (i.e. the distance between the input optode and the detector optode increases). This means that in order to decrease the effect of overlying tissue, larger interoptode spacing should be recommended for NIRS measurements of the brain.

8. Conclusion

We have demonstrated the validity of the modified Beer–Lambert law in an inhomogeneous medium both by analytical proof and MC simulation and have shown how to estimate the effective optical pathlengths within an inhomogeneous medium, data which would be needed for the accurate quantitation of NIRS data. As an example of the application of this technique, a two-concentric-sphere model of the head been used to estimate the contribution of the overlying tissues of the skull to the total optical pathlength. Although it is possible to use the model to estimate the effective optical pathlength in the overlying tissue on the adult or infant head, the values obtained must, as yet, be treated with caution since the size of the model is significantly smaller than that of the real head. The contribution of the overlying tissues to the total effective pathlength decreases as the distance between the input optode

and the detector optode increases, and indicates that larger interoptode spacing should be recommended for NIRS measurement of the brain.

Acknowledgments

References

Arridge S R, Cope M and Delpy D T 1992 Theoretical basis for the determination of optical pathlengths in tissue: temporal and frequency analysis *Phys. Med. Biol.* **37** 1531–60

Arridge S R, Schweiger M, Hiraoka M and Delpy D T 1993a Performance of an iterative reconstruction algorithm for near infrared absorption and scatter imaging *Proc. SPIE* **1888** 360–71

—— 1993b A finite element approach for modelling photon transport in tissue *Med. Phys.* **20** 299–309

Arridge S R, van der Zee P, Cope M and Delpy D T 1991 Reconstruction methods for infra-red absorption imaging *Proc. SPIE* **1431** 205–15

Brazy J E, Lewis D V, Mitnick M H and Jöbsis F F 1985 Noninvasive monitoring of cerebral oxygenation in preterm infants: preliminary observations. *Paediatrics* **75** 217–25

Chance B, Maris M, Sorge J and Zhang M Z 1990 A phase modulation system for dual wavelength difference spectroscopy of haemoglobin deoxygenation in tissue. *Proc. SPIE* **1204** 481–91

Cheong W F, Prahl S A and Welch A J 1990 A review of the optical properties of biological tissues *IEEE J. Quantum Electron.* **QE-26** 2166–85

Cope M 1991 The development of a near infrared spectroscopy system and its application for non invasive monitoring of cerebral blood and tissue oxygenation in newborn infant *PhD Thesis* University of London

Cope M, Delpy D T, Reynolds E O R, Wary J, Wyatt J and van der Zee P 1988 Methods of quantitating cerebral near infrared spectroscopy data *Adv. Exp. Med. Biol.* **222** 183–9

Cui W and Ostrander L E 1992 The relationship of surface reflectance measurements to optical properties of layered biological media *IEEE Trans. Biomed. Eng.* **BME-39** 194-201

Delpy D T, Cope M, van der Zee P, Arridge S R, Wray S and Wyatt J S 1988 Estimation of optical pathlength through tissue from direct time of flight measurement *Phys. Med. Biol.* **33** 1433–42

Edwards A D, Wyatt J S, Richardson C E, Delpy D T and Reynolds E O R 1988 Cotside measurement of cerebral blood flow in ill newborn infants by near infrared spectroscopy *Lancet* ii 770–1

Elwell C E, Cope M, Edwards A D, Wyatt J S, Reynolds E O R and Delpy D T 1992 Measurement of cerebral blood flow in adult human using near infrared spectroscopy—methodology and possible errors *Adv. Exp. Med. Biol.* **317** 235–45

Essenpreis M, Elwell C E, Cope M, van der Zee P, Arridge S R and Delpy D T 1993 Spectral dependence of temporal point spread functions in human tissues *Appl. Opt.* **32** 418–25

Essenpreis M, van der Zee P and Mills T N 1991 Monte Carlo modelling of light transport in tissue: the effect of laser coagulation on light distributions *Proc. SPIE* **1524** 7–23

Ferrari M, Marchis C De, Giannini I, Nicola A Di, Agostino R, Nodari S and Bucci G 1986a Cerebral blood volume and haemoglobin oxygen saturation monitoring in neonatal brain by near infrared spectroscopy *Adv. Exp. Med. Biol.* **200** 203–12

Ferrari M, Zanette E, Giannini I, Sideri G,, Fieschi C and Carpi A 1986b Effect of carotid artery compression test on regional cerebral blood volume, haemoglobin oxygen saturation and cytochrome-c-oxidase redox level in cerebrovascular patients *Adv. Exp. Med. Biol.* **200** 213–22

Firbank M, Hiraoka M, Essenpreis M and Delpy D T 1993 Measurement of the optical properties of skull in the wavelength range 650–950 nm *Phys. Med. Biol.* **38** 503–10

Fishkin J B and Gratton E 1993 Propagation of photon-density waves in strongly scattering media containing an absorbing semi-infinite plane bounded by a straight edge *J. Opt. Soc. Am.* A **10** 127–40

Flock S T, Patterson M S, Wilson B C and Wyman D R 1989 Monte Carlo modelling of light propagation in highly scattering tissue—1: Model predictions and comparison with diffusion theory *IEEE Trans. Biomed. Eng.* **BME-39** 194–201

Fox E, Jöbsis F F and Mitnick M H 1985 Monitoring cerebral oxygen sufficiency in anaesthesia and surgery *Adv. Exp. Med. Biol.* **191** 849–54

Graaff R, Koelink M H, de Mul F F M, Zijlstra W G, Dassel A C M and Aarnoudse J G 1993 Condensed Monte Carlo simulations for the description of light transport *Appl. Opt.* **32** 426–34

Haselgrove J C, Schotland J C and Leigh J S 1992 Long-time behaviour of photon diffusion in an absorbing medium: application to time-resolved spectroscopy *Appl. Opt.* **31** 2678–83

Hebden J C and Wong K S 1993 Time-resolved optical tomography *Appl. Opt.* **32** 372–80

Jöbsis F F 1977 Noninvasive, infrared monitoring of cerebral and myocardial oxygen sufficiency and circulatory parameters *Science* **198** 1264–7

Knüttel A, Schmitt J M and Knutson J R 1993 Spatial localization of absorbing bodies by interfering diffusive photon-density waves *Appl. Opt.* **32** 381–9

Patterson M S, Chance B and Wilson B C 1989 Time resolved reflectance and transmittance for the non invasive measurement of tissue optical properties *Appl. Opt.* **28** 2331–6

Patterson M S, Wilson B C and Wyman D R 1991 The propagation of optical radiation in tissue 1. Models of radiation transport and their application *Lasers Med. Sci.* **6** 155–68

Schweiger M, Arridge S R, Hiraoka M and Delpy D T 1992 Application of the finite element method for the forward model in infra-red absorption imaging *Proc. SPIE* **1768** 97–108

Sevick E M and Chance B 1991 Photon migration in a model of the head measured using time- and frequency-domain techniques: potentials of spectroscopy and imaging *Proc. SPIE* **1431** 84-96

Skov L, Pryds O and Greisen G 1991 Estimating cerebral blood flow in newborn infants: comparison of near infrared spectroscopy and Xe clearance *Paediat. Res.* **30** 570–73

van der Zee P 1993 Measurement and modelling of optical properties of human tissue in the near infrared *PhD Thesis* University of London

van der Zee P, Arridge S R, Cope M and Delpy D T 1990 The effect of optode positioning on optical pathlength in near infrared spectroscopy of brain *Adv. Exp. Med. Biol.* **277** 79–84

van der Zee P, Cope M, Arridge S R, Essenpreis M, Potter L A, Edwards A D, Wyatt J S, McCormick D C, Roth S C, Reynolds E O R and Delpy D T 1992 Experimentally measured optical pathlengths for the adult head, calf and forearm and head of the newborn infant as a function of inter optode spacing *Adv. Exp. Med. Biol.* **316** 143–53

van der Zee P and Delpy D T 1987 Simulation of the point spread function for light in tissue by a Monte Carlo technique *Adv. Exp. Med. Biol.* **215** 179–91

Wilson B C and Adam G 1983 A Monte Carlo model for the absorption and flux distributions of light in tissue *Med. Phys.* **10** 824–30

Wyatt J S, Cope M, Delpy D T, Richardson C E, Edwards A D, Wray S C and Reynolds E O R 1990 Quantitation of cerebral blood volume in newborn infants by near infrared spectroscopy *J. Appl. Phys.* **68** 1086–91

Wyatt J S, Cope M, Delpy D T, Wray S and Reynolds E O R 1986 Quantitation of cerebral oxygenation and haemodynamics in sick newborn infants by near infrared spectroscopy *Lancet* **ii** 1063–6